

# Does the bottomonium counterpart of $X(3872)$ exist?

Zhi-Yong Zhou\* and Dian-Yong Chen†

*School of Physics, Southeast University, Nanjing 211189, P. R. China*

Zhiguang Xiao‡

*Interdisciplinary Center for Theoretical Study,*

*University of Science and Technology of China, Hefei, Anhui 230026, China*

(Dated: October 9, 2018)

## Abstract

Using the extended Friedrichs scheme, we study the bottomonium counterpart of  $X(3872)$ ,  $X_b$ . In this scheme, a dynamically generated virtual state below the  $B\bar{B}^*$  threshold is found, and there is a narrow lineshape peak at about 10615 MeV, just above the threshold in  $B\bar{B}^* \rightarrow B\bar{B}^*$ . However, we find that the virtual state is not the main reason for the peak but it is the form factor, which comes from the convolution of the interaction term and meson wave functions including the one from  $\chi_{b1}(4P)$ , that is responsible for the peak. The form factor also affects the lineshape of a dynamically generated broad resonance with its mass and width at about 10672 MeV and 78 MeV, respectively, and suppresses the magnitude of the peak generated by  $\chi_{b1}(4P)$  with its mass and width being about 10771 MeV and 6 MeV. This study emphasizes the importance of the structure of the wave functions of high radial excitations in the analysis of the lineshapes, and provides a caveat that some signals may be generated from the structures of the form factors rather than from poles.

After the famous enigmatic  $X(3872)$  was observed in 2003 [1], a series of exotic  $XYZ$  states were reported by the experiments in the past decades. One interesting property of these states, such as the  $Z_c$ 's [2, 3],  $Z_b$ 's [4], like the  $X(3872)$ , is their closeness to the nearby thresholds such as  $D^{(*)}\bar{D}^*$  or  $B^{(*)}\bar{B}^*$ , which also inspires the speculations that they are hadron molecules bounded by the long-range force of one pion exchange (OPE), similar to the deuteron in the triplet  $np$  system [5, 6]. In fact, dating back to 1991, by generalizing this OPE mechanism from the  $np$  system to two-heavy-meson systems, some bound states below their corresponding two-heavy-meson thresholds were predicted by Törnqvist [7], especially a bound state just below the  $D\bar{D}^*$  threshold which is close to the  $X(3872)$  mass. Although the meson-exchange mechanism is popular in understanding the appearance of the hadron molecules, the production in hard process of proton and anti-proton colliders [8–10] implies that the  $X(3872)$  may contain a short-distance  $c\bar{c}$  core. Thus, the idea of regarding the  $X(3872)$  as a mixture of  $c\bar{c}$  and  $D\bar{D}^*$  gradually attracts the attention of the community, as reviewed in refs. [11–14].

Due to the heavy quark symmetry, a natural question is where the counterpart of  $X(3872)$  in the bottomonium sector, dubbed the  $X_b$  [15], is. In the literature, the OPE mechanism predicts that the  $B\bar{B}^*$  system is more strongly bounded than the  $D\bar{D}^*$  system. A binding energy of about 42 MeV for the  $B\bar{B}^* + B^*\bar{B}$  system of  $J^{PC} = 1^{++}$  was obtained in refs. [16, 17], which means that the bound state is located at about 10562 MeV. The

existence of a bound state around the  $B\bar{B}^*$  threshold was also qualitatively predicted by considering the isospin exchange mechanism in Ref.[18] and a further calculation predicted the  $X_b$  mass to be 10585 MeV [19]. However, according to the experiences in the calculations of the  $X(3872)$ , the meson exchange forces depend a lot on the chosen types of the exchanged mesons and on the cut-off introduced in regulating the high energy behavior of the interaction [20, 21]. Another method to calculate the properties of  $X_b$  is the effective field theory (EFT). It seems that the EFT method with the heavy quark symmetry are not sufficient to make a prediction of a molecular bound state in the  $B\bar{B}^*$  system [22].

In this paper, we investigate this problem in an alternative approach based on an extended Friedrichs scheme [23–25] proposed by us in recent years. In this picture, the  $X(3872)$  is dynamically generated as a mixture of the  $c\bar{c}$  core and  $D\bar{D}^*$  continuum. This scheme has proved to be successful in understanding the peculiar properties of  $X(3872)$  in studying the charmonium-like spectrum [26, 27] by incorporating the Godfrey-Isgur (GI) model [28] and the quark pair creation (QPC) model [29, 30]. One of the merits in applying the extended Friedrichs scheme in understanding the first excited charmonium states is that there is only one free parameter,  $\gamma$ , the quark pair creation strength, in the calculation. We will use this scheme to study the  $X_b$  state by coupling the  $\chi_{b1}(4P)$  with  $B\bar{B}^* + B^*\bar{B}$  and  $B^*\bar{B}^*$ . We find that a virtual state is dynamically generated below the  $B\bar{B}^*$  threshold and the lineshape just above the threshold has a peak structure, which seems to indicate that there is an  $X_b$  virtual state generating a peak structure. However, by careful analysis, we will show that this peak structure is not contributed mainly by the virtual state but by the form factor in the amplitude.

\* zhouzhy@seu.edu.cn

† chendy@seu.edu.cn

‡ xiaozg@ustc.edu.cn

It is reasonable that the form factor which comes from the convolution of the meson wave functions and interaction terms may have nontrivial structures if higher radial excitations with a few nodes in the wave functions are included. We also show that the lineshape of another dynamically generated broad resonance and magnitude of the lineshape of a narrow resonance which is originated from the  $\chi_{b1}(4P)$  are also largely affected by the structures of the form factors. These results shows that when high radial excitations are involved, the effect of the meson structure is important and may even generate misleading peak signals. A crude use of a Breit-Wigner to fit the peak may not reveal the correct nature of the signal.

Let us first introduce the theoretical background. As proposed in [23, 24], after the angular momentum decomposition and restricted to a specific total angular momentum, the interaction between a discrete state  $|0\rangle$  having a bare energy eigenvalue  $m_0$ , and some continuum two-particle states  $|E; n, SL\rangle$ , where  $E$  is the bare energy eigenvalue in the center of mass system (c.m.s) and  $n, S, L$  denote the species, total spin and total orbital angular momentum, respectively, can be expressed as a Hamiltonian in the form of a Friedrichs model [23, 31],

$$H = m_0|0\rangle\langle 0| + \sum_{n,S,L} \int_{E_{th,n}}^{\infty} dE |E; n, SL\rangle\langle E; n, SL| + \sum_{n,S,L} \int_{E_{th,n}}^{\infty} dE f_{SL}^n(E) |0\rangle\langle E; n, SL| + h.c. \quad (1)$$

where  $E_{th,n}$  is the threshold energy of the  $n$ -th continuum and  $f_{SL}^n(E)$  represents the coupling form factor of the bare discrete state and the  $n$ -th continuum state. The eigenvalue problem of Eq. (1) could be exactly solved [23, 24], and the scattering matrix element of the initial and final continuum states (the subscript  $i$  and  $f$  include their total spin  $S$  and angular momentum  $L$ ) could be expressed as

$$S_{fi}(E, E') = \delta(E - E') \left( \delta_{fi} - 2\pi i \frac{f_i(E) f_f^*(E)}{\eta^+(E)} \right). \quad (2)$$

where the resolvent  $\eta^\pm(x)$  is defined as

$$\eta^\pm(x) = x - m_0 - \sum_{n,S,L} \int_{E_{n,th}}^{\infty} \frac{|f_{SL}^n(E)|^2}{x - E \pm i0} dE. \quad (3)$$

The  $\eta^\pm$  function can be analytically continued to the complex energy plane to be a complex analytic function  $\eta(z)$  for  $z \in \mathbb{C}$  with its boundary values  $\eta(x \pm i0) = \eta^\pm(x)$  on the real axis. Every continuum integral will contribute a discontinuity for the  $\eta(z)$  function and doubles the number of Riemann sheets. For example, in a two-channel case, there are two thresholds,  $a_1$  and  $a_2$ . The physical region between  $a_1$  and  $a_2$  is attached to the second sheet, and the physical region above  $a_2$  is attached to the third Riemann sheet. The solutions for  $\eta(z) = 0$  on the unphysical Riemann sheets will be the poles for

the  $S$ -matrix, which represent the generalized eigenstates with complex eigenvalues (called Gamow state) for the full Hamiltonian [32, 33]. The wave functions of different poles could be explicitly written down [23, 24]. In general, only the poles on the Riemann sheets closest to the physical region will significantly contribute to the observables such as the cross sections or scattering amplitudes.

Once  $m_0$  and  $f_{SL}^n$  are determined, the scattering amplitude and the poles are all determined. A simple method is to use the QPC model [29, 30] to describe the interaction between one meson and two-meson continuum states. The transition operator  $T$  in the QPC model for the  $A \rightarrow BC$  process is defined as

$$T = -3\gamma \sum_m \langle 1m1 - m|00 \rangle \int d^3\vec{p}_3 d^3\vec{p}_4 \delta^3(\vec{p}_3 + \vec{p}_4) \mathcal{Y}_1^m\left(\frac{\vec{p}_3 - \vec{p}_4}{2}\right) \chi_{1-m}^{34} \phi_0^{34} \omega_0^{34} b_3^\dagger(\vec{p}_3) d_4^\dagger(\vec{p}_4), \quad (4)$$

describing the process of a quark-antiquark pair being generated by the  $b_3^\dagger$  and  $d_4^\dagger$  creation operators from the vacuum.  $\phi_0^{34} = (u\bar{u} + d\bar{d} + s\bar{s})/\sqrt{3}$  is the  $SU(3)$  flavor wave function for the quark-antiquark pair.  $\chi_{1-m}^{34}$  and  $\omega_0^{34}$  are the spin wave function and the color wave function, respectively.  $\mathcal{Y}_1^m$  is the solid Harmonic function.  $\gamma$  parameterizes the production strength of the quark-antiquark pair from the vacuum. The definition of the meson mock state here reads

$$|A(n_r, {}^{2s+1}l_j)(\vec{P})\rangle = \sum_{m_l, m_s} \langle l m_l s m_s | j m \rangle \int d^3p \psi_{n_r, l m_l}(\vec{p}) \times \chi_{s m_s}^{12} \phi^{12} \omega^{12} \left| q_1 \left( \frac{m_1}{m_1 + m_2} \vec{P} + \vec{p} \right) \bar{q}_2 \left( \frac{m_2}{m_1 + m_2} \vec{P} - \vec{p} \right) \right\rangle.$$

$\chi^{12}$ ,  $\phi^{12}$  and  $\omega^{12}$  are the spin wave function, flavor wave function and the color wave function, respectively.  $p_1$  ( $p_2$ ) and  $m_1$  ( $m_2$ ) are the momentum and mass of the quark (anti-quark).  $\vec{P} = \vec{p}_1 + \vec{p}_2$  is the momentum of the center of mass, and  $\vec{p} = \frac{m_2 \vec{p}_1 - m_1 \vec{p}_2}{m_1 + m_2}$  is the relative momentum.  $\psi_{n_r, l m_l}$  is the wave function for the bare meson state, with  $n_r$  being the radial quantum number,  $l$  the relative angular momentum of the quark and anti-quark, and  $m_l$  its third component.

By the standard derivation one can obtain the coupling form factor between  $|A\rangle$  and  $|BC\rangle$  in the Friedrichs model by  $f_{SL}(E) = \sqrt{\mu p} \mathcal{M}^{SL}(p)$ , where  $\mu$  is the reduced mass,  $p = \sqrt{\frac{2M_B M_C (E - M_B - M_C)}{M_B + M_C}}$  is the momentum of  $B$  or  $C$  in their c.m.s.,  $M_B$  and  $M_C$  being the masses of meson  $B$  and  $C$  respectively, and  $\mathcal{M}^{SL}$  is the  $L$ -partial wave amplitude with the total spin  $S$  of the two-particle state.

When the wave functions and the masses of the bare states are given, the form factor  $f_{SL}$  can be obtained, and thus, from Eq. (2), the scattering amplitudes of the particular channels can be obtained and the bound states, virtual states or resonant states could be solved from  $\eta^{nth \text{ sheet}}(z) = 0$  on the  $n$ th Riemann sheet. The  $G(z) \equiv f_i(z) f_f^*(z)$  in Eq. (2) will be called residue function in the following.

We will use the GI model to supply the wave functions and the mass of the bare state, because it has been

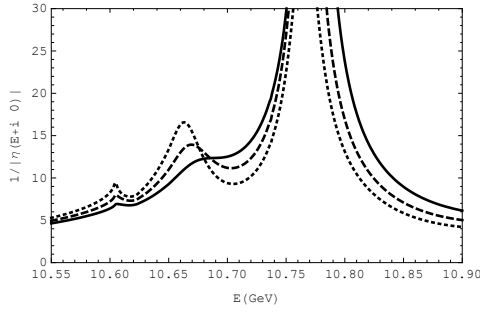


FIG. 1.  $|\frac{1}{\eta(E+i0)}|$  on the real axis with  $\gamma = 4.0$ (solid), 4.9(dashed), and 5.6(dotted), respectively.

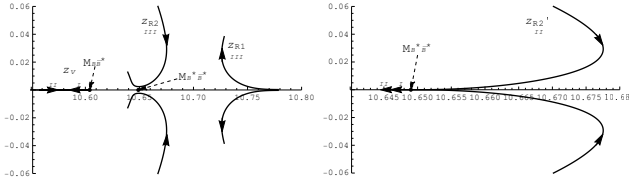


FIG. 2. The trajectories of poles on the complex energy plane as  $\gamma$  increases. The *I*, *II*, and *III* denote the sheet numbers of the poles as described in the text. Left:  $z_v$ ,  $z_{R1}$ , and  $z_{R2}$  with both  $B\bar{B}^*$  and  $B^*\bar{B}^*$  continua. Right:  $z'_{R2}$  poles with only the  $B^*\bar{B}^*$ .

proved globally successful in predicting meson states below the open-flavor thresholds. The predicted mass of  $\chi_{b1}(4P)$  by GI is about 10790 MeV. Since the  $B\bar{B}^*$  channel opens above about 10604 MeV and the  $B^*\bar{B}^*$  channel opens above 10649 MeV, it is natural to conjecture that the  $\chi_{b1}(4P)$  state will couple to the open  $B^0\bar{B}^{0*} + h.c.$ ,  $B^+\bar{B}^{-*} + h.c.$ , and  $B^{0*}\bar{B}^{0*} + B^{+*}\bar{B}^{-*}$  channels.

The wave functions of  $B$ ,  $B^*$ , and  $\chi_{b1}(4P)$  could be obtained from the GI model with all the model parameters fixed at their original values [28]. Then, the only undetermined parameter in our calculation,  $\gamma$ , is chosen at about  $\gamma = 4.0$ , where the  $X(3872)$  and the first excited charmonium states could be reproduced simultaneously [26, 27]. By solving the zero points of  $\eta(z)$ , three states are found near the physical region: a virtual-state pole on the second Riemann sheet below the  $B\bar{B}^*$  threshold at  $z_v = 10593$  MeV, a pair of conjugate poles at  $z_{R1} = 10771 \pm 3i$  MeV on the third Riemann sheet and another pair of third-sheet conjugate poles at  $z_{R2} = 10672 \pm 39i$  MeV. From the curves of  $|\frac{1}{\eta(E+i0)}|$  in Fig.1, one can see that the virtual state pole contributes a small cusp at the  $B\bar{B}^*$  threshold, while the other two states contribute two peaks around the corresponding energies.

One may wonder where these states come from. Their origins could be revealed by tracking their pole trajectories along with the change of  $\gamma$ , as indicated in Fig. 2. As  $\gamma$  becomes smaller, the virtual-state pole  $z_v$  moves down towards the negative infinity on the real axis, remain-

ing as a virtual state. Conversely, if  $\gamma$  is turned larger, the virtual state will move up along the real axis and reach the threshold at  $\gamma \simeq 8.5$ , and then it will come up to the first sheet becoming a bound state. This kind of behavior is the typical behavior for dynamically generated states in  $S$ -wave with attractive interaction [25]. Therefore, the state can be viewed as dynamically generated mainly from the  $S$ -wave interaction between the bare  $\chi_{b1}(4P)$  state and  $B\bar{B}^*$  continuum.

As  $\gamma$  becomes smaller and at last is turned off, the  $z_{R1}$  pole moves to the position of the bare state  $\chi_{b1}(4P)$ . This reveals that this state is originated from the bare  $\chi_{c1}(4P)$  state and obtains a width of about 6 MeV by coupling to the open thresholds when  $\gamma = 4.0$ .

The behavior of the  $z_{R2}$  pole is a little complicated. As  $\gamma$  increases, the  $z_{R2}$  pole pair on the third sheet will come close to the  $B^*\bar{B}^*$  threshold but will not reach the real axis. When  $\gamma$  becomes large enough and the real part of the pole is roughly below the  $B^*\bar{B}^*$  threshold, they will separate and move apart on the complex plane as shown in Fig. 2. The origin of  $z_{R2}$  could be clarified by switching off the interaction with the  $B\bar{B}^*$ . If  $\chi_{b1}(4P)$  only interacts with the  $B^*\bar{B}^*$  continuum, there will be only one cut and two Riemann sheets. As the interaction becomes stronger, the  $z'_{R2}$  poles, which correspond to the third-sheet  $z_{R2}$  poles in two-continuum case, will move towards the  $B^*\bar{B}^*$  threshold and merge with the threshold there, and then they move separately onto the real axis on different Riemann sheets, becoming a bound state pole and a virtual state pole, as shown in Fig. 2. This kind of pole trajectory is typical for the states in higher partial waves with attractive interaction. On the contrary, if we keep the interaction between  $\chi_{b1}(4P)$  and  $B\bar{B}^*$ , the pole just moves on the complex plane when  $\gamma$  changes. Therefore, we conclude that the  $z_{R2}$  is mainly generated from the interaction between  $\chi_{b1}(4P)$  with  $B^*\bar{B}^*$ .

Thus, it is because the  $S$ -wave interaction plays a crucial role in the formation of  $z_v$  and the  $D$ -wave interaction is responsible for the formation of  $z_{R2}$  that the behaviors of these two dynamically generated poles,  $z_{R2}$  and  $z_v$ , are different.

The scattering process of the continuum states is described by Eq. (2). As shown in Fig. 3,  $|T_{B\bar{B}^* \rightarrow B\bar{B}^*}|^2$  exhibits a very narrow peak in the lineshape just above the threshold. If this peak is able to be observed in the experiments and its lineshape is blindly fitted with a Breit-Wigner formula, it will be concluded that there is a state with a mass about 10615 MeV and a width about 15 MeV by a rough estimation. However, as we have shown, there is no such a zero point of the resolvent function and one can hardly imagine that the virtual state at  $z_v$ , about 10 MeV below the threshold on the second sheet, can generate such a narrow structure near the threshold. In fact, this lineshape peak is mainly contributed by the residue function in Eq. (2), i.e. the  $\sum_{SL} |f_{SL}^n(E)|^2$  terms, but not by the virtual state. This statement can be clarified by comparing the  $|1/\eta|$  behavior in Fig. 1 and the residue function behavior in Fig.3. Even though  $\gamma$  is in-

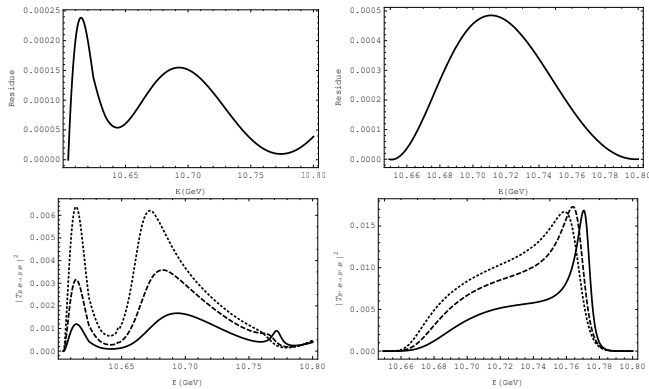


FIG. 3. The residue functions of  $B\bar{B}^*$  (left) and  $B^*\bar{B}^*$  (right) are shown in the first row. The absolute square of scattering amplitudes of  $BB^*$  and  $B^*B^*$  with  $\gamma = 4.0$  (solid), 4.9 (dashed), and 5.6 (dotted), respectively, are shown in the second row.

creased to about 5.6, the virtual-state pole will move to 10600 MeV and its contribution to the threshold enhancement for  $|1/\eta|$  is still not significant as shown in Fig. 1. Only if  $\gamma$  is tuned up to 8.0, about twice of the original 4.0, when the virtual state comes fairly close to the  $B\bar{B}^*$  threshold, its contribution will be significant. However, the residue function behavior shown in Fig.3 presents a peak just around the peak in  $|T|^2$ . Since the coupling function  $f_{SL}^n(E)$  in the residue function is obtained from the QPC model and thus comes from the overlap of the meson wave functions. For mesons with higher radial quantum number, such as  $\chi_{b1}(4P)$  here, there would be more nodes in the radial wave function of the mesons. Therefore, one can imagine that it is possible to generate some wavy structure like in  $B\bar{B}^*$  scattering in Fig. 3 after the convolution of three meson wave functions and the interactions.

In the  $B^*\bar{B}^*$  scattering,  $z_{R2}$  and the residue function together will contribute a bump structure, which also appears in the  $B\bar{B}^*$  scattering. The residue function also plays a role in this structure. The  $z_{R2}$  has a broad width of about 78MeV at  $\gamma = 4.0$ , which is expected to be a very mild structure. In  $B\bar{B}^*$  the line shape around this state is much more enhanced than in  $B^*B^*$ . This is because its position is in a sharply rising part of the residue function in  $B\bar{B}^*$ , being closer to the maximum of the bump in the residue function than in  $B^*\bar{B}^*$ , and also because position of the valley of the residue function comes below  $z_{R1}$  in  $B\bar{B}^*$ . Thus, this bump structure gets its shape much more from the residue function than from the pole, which can easily be seen by comparing Fig. 1 and Fig. 3. Even though the  $z_{R1}$  state is a very narrow state which receives less influence from the residue function, a careful observation shows that in the  $B\bar{B}^*$  channel the position

of  $\chi_{b1}(4P)$  state is just inside the valley of residue function, and as a result, its maximum contribution in  $|T|^2$  is comparable to the maximum of the  $z_{R2}$  bump, while in  $B^*\bar{B}^*$ , its peaks is rather sharper and higher compared to the mild structure from  $z_{R2}$ .

In summary, we utilize the extended Friedrichs scheme with the wave functions and spectrum from GI model as input to study the pole structure of  $B\bar{B}^*$  and  $B^*\bar{B}^*$  scatterings by coupling  $\chi_{b1}(4P)$  with  $B\bar{B}^*$  and  $B^*\bar{B}^*$ . In this analysis we demonstrate that when higher radial excitation states are involved in the interaction, the non-trivial structure of the form factor may play an important role in the experimentally observed lineshapes and may generate misleading bump signals. In particular, a near-threshold peak structure appears in  $B\bar{B}^*$  channel, which may be interpreted as the counterpart of  $X(3872)$  in  $B\bar{B}^*$ . However, we have shown that this peak is mainly generated by the residue function in the amplitude constructed from the form factor rather than by a dynamically generated second sheet virtual state near the threshold, around 10593 MeV. A broad dynamically generated resonance with a mass around 10672 MeV and a width around 78 MeV is also found in this system. However, the contribution from this broad resonance to the line shape is also largely modified by the residue function. The mass and width of  $\chi_{c1}(4P)$  is found to be about 10771 MeV and 6 MeV, respectively. The relative magnitude of the peak generated by this narrow resonance may also be suppressed by a valley of the residue function. The nontrivial structure in the form factor is closely related to the nodes in the meson wave functions for high radial excitations. Thus, the precise structures of the meson wave functions would play more and more important roles when the radial quantum number for the states involved become larger and larger. This may also be a reason for the ineffectiveness of the EFT approach in the discussions of the higher radial excitations. In the EFT, the states are assumed to have no internal structures and the information of the form factors is absorbed into the coupling constants. One can imagine that the EFT must go to higher orders to reproduce the nontrivial behaviors of the form factors or must include some form factors inserted by hand without any solid theoretical ground, which may constrain the effectiveness of the theory.

## ACKNOWLEDGMENTS

Z.Z is supported by the Natural Science Foundation of Jiangsu Province of China under contract No. BK20171349. D.C. is supported by China National Natural Science Foundation under contract No. 11775050. Z.X. is supported by China National Natural Science Foundation under contract No. 11105138, 11575177 and 11235010.

- 
- [1] S. K. Choi *et al.* (Belle Collaboration), Phys. Rev. Lett., **91**, 262001 (2003), arXiv:hep-ex/0309032 [hep-ex].
- [2] M. Ablikim *et al.* (BESIII), Phys. Rev. Lett., **110**, 252001 (2013), arXiv:1303.5949 [hep-ex].
- [3] M. Ablikim *et al.* (BESIII), Phys. Rev. Lett., **112**, 132001 (2014), arXiv:1308.2760 [hep-ex].
- [4] A. Bondar *et al.* (Belle), Phys. Rev. Lett., **108**, 122001 (2012), arXiv:1110.2251 [hep-ex].
- [5] S. Weinberg, Phys. Rev., **130**, 776 (1963).
- [6] S. Weinberg, Phys. Rev., **137**, B672 (1965).
- [7] N. A. Törnqvist, Phys. Rev. Lett., **67**, 556 (1991).
- [8] D. Acosta *et al.* (CDF), Phys. Rev. Lett., **93**, 072001 (2014), arXiv:hep-ex/0312021 [hep-ex].
- [9] V. M. Abazov *et al.* (D0), Phys. Rev. Lett., **93**, 162002 (2004), arXiv:hep-ex/0405004 [hep-ex].
- [10] R. Aaij *et al.* (LHCb), Eur. Phys. J., **C72**, 1972 (2012), arXiv:1112.5310 [hep-ex].
- [11] F.-K. Guo, C. Hanhart, U.-G. Meißner, Q. Wang, Q. Zhao, and B.-S. Zou, Rev. Mod. Phys., **90**, 015004 (2018), arXiv:1705.00141 [hep-ph].
- [12] H.-X. Chen, W. Chen, X. Liu, and S.-L. Zhu, Phys. Rept., **639**, 1 (2016), arXiv:1601.02092 [hep-ph].
- [13] R. F. Lebed, R. E. Mitchell, and E. S. Swanson, Prog. Part. Nucl. Phys., **93**, 143 (2017), arXiv:1610.04528 [hep-ph].
- [14] A. Esposito, A. Pilloni, and A. Polosa, Physics Reports, **668**, 1 (2017), ISSN 0370-1573, multiquark Resonances.
- [15] W.-S. Hou, Phys. Rev., **D74**, 017504 (2006), arXiv:hep-ph/0606016 [hep-ph].
- [16] N. A. Tornqvist, Z. Phys., **C61**, 525 (1994), arXiv:hep-ph/9310247 [hep-ph].
- [17] E. S. Swanson, Phys. Rept., **429**, 243 (2006), arXiv:hep-ph/0601110 [hep-ph].
- [18] M. Karliner and J. L. Rosner, Phys. Rev. Lett., **115**, 122001 (2015), arXiv:1506.06386 [hep-ph].
- [19] M. Karliner and S. Nussinov, JHEP, **07**, 153 (2013), arXiv:1304.0345 [hep-ph].
- [20] Y.-R. Liu, X. Liu, W.-Z. Deng, and S.-L. Zhu, Eur. Phys. J., **C56**, 63 (2008), arXiv:0801.3540 [hep-ph].
- [21] N. Li and S.-L. Zhu, Phys. Rev. D, **86**, 074022 (2012).
- [22] A bound state at 10604 MeV was presented in an unpublished version of ref. [34].
- [23] Z. Xiao and Z.-Y. Zhou, J. Math. Phys., **58**, 072102 (2017), arXiv:1610.07460 [hep-ph].
- [24] Z. Xiao and Z.-Y. Zhou, J. Math. Phys., **58**, 062110 (2017), arXiv:1608.06833 [hep-ph].
- [25] Z. Xiao and Z.-Y. Zhou, Phys. Rev., **D 94**, 076006 (2016), arXiv:1608.00468 [hep-ph].
- [26] Z.-Y. Zhou and Z. Xiao, Phys. Rev., **D96**, 054031 (2017), [Erratum: Phys. Rev. D 96, 099905 (2017)], arXiv:1704.04438 [hep-ph].
- [27] Z.-Y. Zhou and Z. Xiao, (2017), arXiv:1711.01930 [hep-ph].
- [28] S. Godfrey and N. Isgur, Phys. Rev., **D 32**, 189 (1985).
- [29] L. Micu, Nucl. Phys., **B10**, 521 (1969).
- [30] H. G. Blundell and S. Godfrey, Phys. Rev., **D 53**, 3700 (1996), arXiv:hep-ph/9508264 [hep-ph].
- [31] K. O. Friedrichs, Commun. Pure Appl. Math., **1**, 361 (1948).
- [32] A. Bohm and M. Gadella, *Dirac Kets, Gamow Vectors and Gel'fand Triplets*, edited by A. Bohm and J. D. Dollard, Lecture Notes in Physics, Vol. 348 (Springer Berlin Heidelberg, 1989) ISBN 978-3-540-51916-4 (Print) 978-3-540-46859-2 (Online).
- [33] O. Civitarese and M. Gadella, Phys. Rep., **396**, 41 (2004), ISSN 0370-1573.
- [34] M. T. AlFiky, F. Gabbiani, and A. A. Petrov, Phys. Lett., **B640**, 238 (2006), arXiv:hep-ph/0506141 [hep-ph].